STELLAR SPECTRA

B. LTE Line Formation

R.J. Rutten

Lingezicht Astrophysics, Deil
Institutt for Teoretisk Astrofysikk, Oslo

October 27, 2013

Contents

Introduction

These three exercises treat the formation of spectral lines in the solar atmosphere assuming Local Thermodynamical Equilibrium (LTE). The topics are:

- *stratification of the solar atmosphere*;

- *formation of the continuous solar spectrum*;

- *formation of Fraunhofer lines in the solar spectrum*.

The method consists of experimentation using IDL. The exercises require knowledge of basic radiative transfer.

These exercises are a sequel to the exercises *"Stellar Spectra A: Basic Line Formation"*. The two sets are independent in the sense that you don't have to have worked through the first set to do the present set. However, various concepts needed in the present set are treated in the second and third exercises of the first set and some of the programs constructed there are useful here, so that it may be of interest to you to go through these quickly. They are found at `http://www.staff.science.uu.nl/~rutte101/rrweb/rjr-edu/exercises/ssa`.

Your report on these exercises should include pertinent graphs made with your own IDL (or with Python's numpy, which becomes a worthy public-domain successor to IDL). My "Simple IDL instruction of astronomy students" is available at `http://www.staff.science.uu.nl/~rutte101/Recipes_IDL.html`.

A template for writing your report and a simple manual for its production with LaTeX and BibTeX are available at `http://www.staff.science.uu.nl/~rutte101/Report_recipe.html`.

These also show how to produce in-text citations that open the corresponding ADS abstract page in a browser when you click on them in a pdf reader such as Acrobat (as holds for the citations in this instruction; I also added such ADS links to the reference list although that is effectively superfluous in on-screen reading).

Table 1: *Selected units and constants. Precise values available at `http://physics.nist.gov/cuu/Constants/index.html`.*

$1\,\text{Å} = 0.1\,\text{nm} = 10^{-8}\,\text{cm}$

$1\,\text{erg} = 10^{-7}\,\text{Joule}$

$1\,\text{dyne cm}^{-2} = 0.1\,\text{Pascal} = 10^{-6}\,\text{bar} = 9.8693 \times 10^{-7}\,\text{atmosphere}$

energy of $1\,\text{eV} = 1.60219 \times 10^{-12}\,\text{erg}$

photon energy (in eV) $E = 12398.55/\lambda$ (in Å)

speed of light $c = 2.99792 \times 10^{10}\,\text{cm s}^{-1}$

Planck constant $h = 6.62607 \times 10^{-27}\,\text{erg s}$

Boltzmann constant $k = 1.38065 \times 10^{-16}\,\text{erg K}^{-1}$
$\qquad\qquad\quad = 8.61734 \times 10^{-5}\,\text{eV K}^{-1}$

electron mass $m_\text{e} = 9.10939 \times 10^{-28}\,\text{g}$

proton mass $m_\text{p} = 1.67262 \times 10^{-24}\,\text{g}$

atomic mass unit (amu, C=12) $m_\text{A} = 1.66054 \times 10^{-24}\,\text{g}$

first Bohr orbit radius $a_0 = 0.529178 \times 10^{-9}\,\text{cm}$

hydrogen ionization energy $\chi_\text{H} = 13.598\,\text{eV}$

solar mass $M_\odot = 1.9891 \times 10^{33}\,\text{g}$

solar radius $R_\odot = 6.9599 \times 10^{10}\,\text{cm}$

distance sun – earth $AE = 1.49598 \times 10^{13}\,\text{cm}$

earth mass $M_\oplus = 5.976 \times 10^{27}\,\text{g}$

earth radius $R_\oplus = 6.3710 \times 10^{8}\,\text{cm}$

1 Stratification of the solar atmosphere

In this exercise you study the radial stratification of the solar atmosphere on the basis of the standard model FALC by Fontenla et al. (1993). They derived this description of the solar photosphere and chromosphere empirically, assuming that the solar atmosphere is horizontally homogeneous ("plane parallel layers") and in hydrostatic equilibrium ("time independent").

Figure 1: *Eugene H. Avrett (born 1933) represents the A in the VAL (Vernazza, Avrett and Loeser) and FAL (Fontenla, Avrett and Loeser) sequences of standard models of the solar atmosphere. At the Center for Astrophysics (Cambridge, Mass.) he developed, together with programmer Rudolf Loeser, an enormous spectrum modeling code (called Pandora, perhaps a fitting name) which fits observed solar continua and lines throughout the spectrum through the combination of trial-and-error adjustment of the temperature stratification with simultaneous evaluation of the corresponding particle densities with great sophistication, basically performing complete NLTE population analysis for all key transitions in the solar spectrum. His VALIII paper (Vernazza et al. 1981) stands as one of the three prime solar physics papers of the second half of the twentieth century (with Parker's 1958 solar wind prediction and Ulrich's 1970 p-mode prediction). His latest model is described in Avrett & Loeser (2008) Photograph from the web.*

The FALC model is specified in Tables 3–4 and in file `falc.dat`[1]. Copy this file to your work directory.
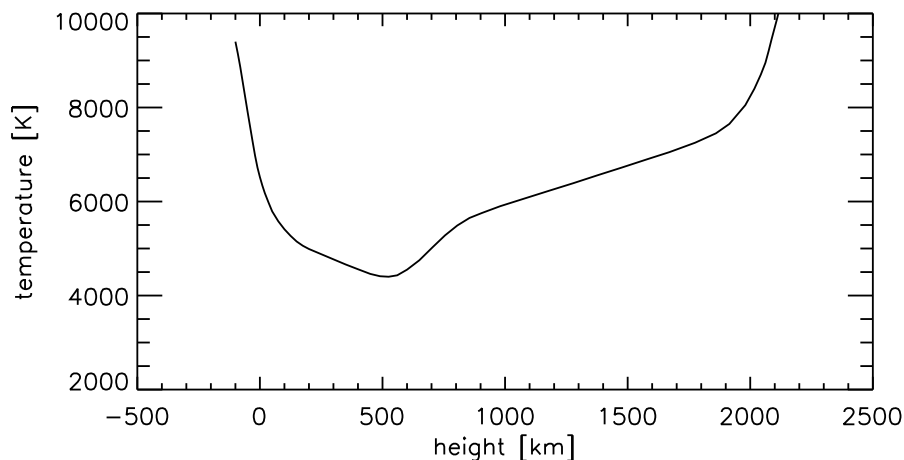
Figure 2: *Temperature stratification of the FALC model. The height scale has h = 0 at the location with $\tau_{500} = 1$. The photosphere reaches until h = 525 km (temperature minimum). The chromosphere higher up has a mild temperature rise out to h ≈ 2100 km where the steep increase to the 1–2 MK corona starts ("transition region").*

---

[1] At http://www.staff.science.uu.nl/~rutte101/rrweb/rjr-edu/exercises/ssb/, together with other IDL input files and with my own graphical output of these exercises as files `ssb_answers`.

3

The first column in Tables 3–4 specifies the height h which is the distance above $\tau_{500} = 1$ where τ_{500}, given in the second column, is the radial optical depth in the continuum at $\lambda = 500$ nm. The quantity m in the third column is the mass of a column with cross-section 1 cm^2 above the given location.

In the photosphere ($-100 \leq h \leq 525$ km) and chromosphere ($525 \leq h \leq 2100$ km) the temperature T (fourth column) has been adjusted empirically so that the computed spectrum is in agreement with the spatially averaged disk-center spectrum observed from quiet solar areas (away from active regions). The temperature distribution in the transition region (above $h \approx 2100$ km, up to $T = 10^5$ K) has been determined theoretically by balancing the downflow of energy from the corona through thermal conduction and diffusion against the radiative energy losses.

The microturbulent velocity v_t roughly accounts for the Doppler broadening that is observed to exceed the thermal broadening of lines formed at various heights. The total pressure P_{tot} is the sum of the gas pressure P_{gas} and the corresponding turbulent pressure $\rho\, v_t^2 / 2$ where ρ is the gas density (last column).

The tables also lists the total hydrogen density n_{H}, the free proton density n_{p}, and the free electron density n_{e}. Given the T and v_t distributions with height, these number densities and other quantities were determined by requiring hydrostatic equilibrium and evaluating the ionization balances by solving the coupled radiative transfer and statistical equilibrium equations (without assuming LTE). The adopted helium-to-hydrogen abundance ratio is $N_{\text{He}}/N_{\text{H}} = 0.1$. The relative abundances of the other elements came from Anders & Grevesse (1989). Nowadays one would use those of Asplund et al. (2009).

1.1 FALC temperature stratification

Figure 2 shows the FALC temperature stratification. It was made with IDL code similar to the following:

```
; read falc model
close,1
openr,1,'falc.dat'
dummy=''
for iskip=1,4 do readf,1,dummy    ; skip header lines
nh=80                ; nr FALC height values
falc=fltarr(11,nh)   ; 11 FALC columns

readf,1,falc                 ; basic (cumbersome) IDL table reading
h=reform(falc[0,*])          ; reform strips empty dimensions
tau5=reform(falc[1,*])
colm=reform(falc[2,*])
temp=reform(falc[3,*])
vturb=reform(falc[4,*])
nhyd=reform(falc[5,*])
nprot=reform(falc[6,*])
nel=reform(falc[7,*])
ptot=reform(falc[8,*])
pgasptot=reform(falc[9,*])
dens=reform(falc[10,*])

readcol,'falc.dat',h,tau5,colm,temp,vturb,nhyd,nprot,nel,ptot,$
  pgasplot,dens,skipline=4  ; much easier alternative using an astrolib routine
```

4

```
; plot falc model
plot,h,temp,yrange=[3000,10000],$
  xtitle='height [km]',ytitle='temperature [K]'

; repeat plot on postscript file
set_plot,'ps'        ; repeat plot on PostScript file
device,filename='falc_temp_height.ps'
plot,h,temp,yrange=[3000,10000],$
  xtitle='height [km]',ytitle='temperature [K]'
device,/close
set_plot,'x'         ; return to screen; set_plot,'win' for Windows
end
```

- Write similar code and make it work.

1.2 FALC density stratification

We will now study relations between various FALC model parameters. This is easiest done by trying out plots on the IDL command line after running an IDL main program such as the one above. You will often need to generate logarithmic axes with keywords /xlog and /ylog in command plot, and you will also need keyword \ynozero to plot y-axes without extension down to $y = 0$. Various constants are specified in Table 1 on page 2.

- Plot the total pressure p_{total} against the column mass m, both linearly and logarithmically. You will find that they scale linearly. Explain what assumption has caused $p_{\text{total}} = c\,m$ and determine the value of the solar surface gravity $g_{\text{surface}} = c$ that went into the FALC-producing code.

- Fontenla et al. (1993) also assumed complete mixing, i.e., the same element mix at all heights. Check this by plotting the ratio of the hydrogen mass density to the total mass density against height (the hydrogen atom mass is $m_{\text{H}} = 1.67352 \times 10^{-24}$ g, e.g., Allen 1976). Then add helium to hydrogen using their abundance and mass ratios ($N_{\text{He}}/N_{\text{H}} = 0.1$, $m_{\text{He}} = 3.97\,m_{\text{H}}$), and estimate the fraction of the total mass density made up by the remaining elements in the model mix (the "metals").

- Plot the column mass against height. The curve becomes nearly straight when you make the y-axis logarithmic. Why is that? Why isn't it exactly straight?

- Plot the gas density against height. Estimate the density scale height H_ρ in $\rho \approx \rho(0)\exp(-h/H_\rho)$ in the photosphere.

- Compute the gas pressure and plot it against height. Overplot the product $(n_{\text{H}} + n_{\text{e}})\,kT$. Plot the ratio of the two curves to show their differences. Do the differences measure deviations from the ideal gas law or something else? Now add the helium density N_{He} to the product and enlarge the deviations. Comments?

- Plot the total hydrogen density against height and overplot curves for the electron density, the proton density, and the density of the electrons that do not result from hydrogen ionization. Explain their behavior. You may find inspiration in Figure 6 on page 13. The last curve is parallel to the hydrogen density over a considerable height range. What does that imply? And what happens at larger height?

5

- Plot the ionization fraction of hydrogen logarithmically against height. Why does this curve look like the one in Figure 2? And why is it tilted with respect to that?

- Let us now compare the photon and particle densities. In thermodynamic equilibrium (TE) the radiation is isotropic with intensity $I_\nu = B_\nu$ and has total energy density (Stefan Boltzmann)

$$u = \frac{1}{c} \iint B_\nu \, d\Omega \, d\nu = \frac{4\sigma}{c} T^4, \tag{1}$$

so that the total photon density for isotropic TE radiation is given, with $u_\nu = du/d\nu$, T in K and N_{phot} in photons per cm^3, by

$$N_{\text{phot}} = \int_0^\infty \frac{u_\nu}{h\nu} \, d\nu \approx 20 \, T^3. \tag{2}$$

This equation gives a reasonable estimate for the photon density at the deepest model location, why? Compute the value there and compare it to the hydrogen density. Why is the equation not valid higher up in the atmosphere? The photon density there is $N_{\text{phot}} \approx 20 \, T_{\text{eff}}^3 / 2\pi$ with $T_{\text{eff}} = 5770 \, \text{K}$ the effective solar temperature (since $\pi B(T_{\text{eff}}) = \sigma T_{\text{eff}}^3 = \mathcal{F}^+ = \pi \overline{I^+}$ with $\mathcal{F}^+$ the emergent flux and $\overline{I^+}$ the disk-averaged emergent intensity). Compare it to the hydrogen density at the highest location in the FALC model. The medium there is insensitive to these photons (except those at the center wavelength of the hydrogen Lyα line), why?.

1.3   Comparison with the earth's atmosphere

Figure 3 shows the temperature distribution in our own atmosphere. Table 2 specifies its average parameters (the original table in Allen 1976 continues to $h = 50\,000$ km). It is available as file `earth.dat`. Copy this file also to your work directory.

The particle density in the last column is the sum of the molecules, atoms and ions, but neglects free electrons which are indeed negligible below $h \approx 100$ km.
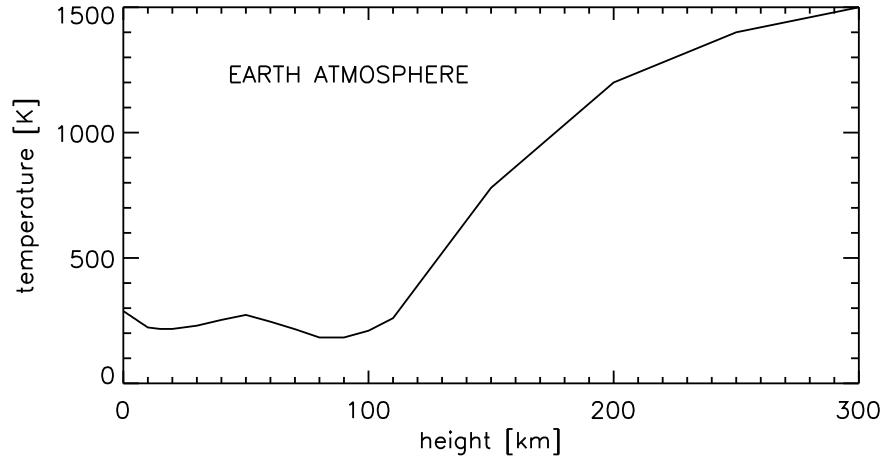
Figure 3: *Temperature stratification of the mean earth atmosphere. The height scale has h = 0 at the earth's surface. Nomenclature: the troposphere ranges until h =11 km, the stratosphere over h = 11 − 47 km, the ionosphere above h = 50 km, with subdivision in the mesosphere (h = 52 − 79 km) and the thermosphere (beyond h = 90 km). The temperature gradient change starting at h = 11 km is called the tropopause, the temperature maximum around h = 50 km the stratopause, the minimum around h = 85 km the mesopause.*

- Write IDL code to read file `earth.dat`.

- Plot the temperature, pressure, particle density and gas density against height, logarithmically where appropriate.

- Plot the pressure and density stratifications together in normalized units in one graph. Comments?

- Plot the mean molecular weight $\mu_E \equiv \overline{m}/m_H = \rho/(N\,m_H)$ against height. Why does it decrease in the high atmosphere?

- Estimate the density scales height of the lower terrestrial atmosphere. Which quantities make it differ from the solar one? How much harder do you have to breathe on Mount Everest?

- Compare the terrestrial parameter values to the solar ones, at the base of each atmosphere. What is the ratio of the particle densities at $h = 0$ in the two atmospheres?

- The standard gravity at the earth's surface is $g_E = 980.665\ \mathrm{cm\,s^{-2}}$. Use this value to estimate the atmospheric column mass $(\mathrm{g\,cm^{-2}})$ at the earth's surface and compare that also to the value at the base of the solar atmosphere.

- Final question: the energy flux of the sunshine reaching our planet ("irradiance") is

$$\mathcal{R} = \frac{4\pi R^2}{4\pi D^2}\,\mathcal{F}_\odot^+ \tag{3}$$

with $\mathcal{F}_\odot^+ = \pi B(T_{\mathrm{eff}}^\odot)$ the emergent solar flux, R the solar radius and D the distance sun–earth, so that the sunshine photon density at earth is

$$N_{\mathrm{phot}} = \pi \frac{R^2}{D^2}\,N_{\mathrm{phot}}^{\mathrm{top}} \tag{4}$$

with $N_{\mathrm{phot}}^{\mathrm{top}}$ the photon density at the top of FALC which you determined at the end of Section 1.1. Compare N_{phot} to the particle density in the air around us, and to the local thermal photon production derived from (2). Comments?

1.4 Discussion

The comparisons between particle density and column mass at the base of the solar photosphere and the base of the earth's atmosphere show that sunlight reaches the earth's surface at a particle density that is much higher than the density at the sunlight $\tau = 1$ escape location within the sun, i.e., the atmospheric depth where the solar gas becomes opaque. If, reversely, the earth were irradiating the sun, that level is where the earthshine would stop already, having passed through a much smaller amount of solar gas then it went through in the nearly transparant earth atmosphere (transmission 80% at $\lambda = 500$ nm at sea level when the sky is clear, (Allen 1976).

Thus, the solar gas is much more opaque per particle than air, even though the terrestrial air particles (molecules) are much larger than the solar atmospheric particles (mostly hydrogen atoms and electrons). In the first decades of the twentieth century the source of this very large opacity was an unsolved riddle as important as the quest for the subatomic energy source that makes the sun shine (for example, see the eloquent last paragraph of Eddington 1926. That opacity is the topic of the next exercise.

Table 2: Earth atmosphere, from Allen (1976).

h	$\log P$	T	$\log \rho$	$\log N$
km	dyn cm^{-2}	K	g cm^{-3}	cm^{-3}
0	6.01	288	–2.91	19.41
1	5.95	282	–2.95	19.36
2	5.90	275	–3.00	19.31
3	5.85	269	–3.04	19.28
4	5.79	262	–3.09	19.23
5	5.73	256	–3.13	19.19
6	5.67	249	–3.18	19.14
8	5.55	236	–3.28	19.04
10	5.42	223	–3.38	18.98
15	5.08	217	–3.71	18.61
20	4.75	217	–4.05	18.27
30	4.08	230	–4.74	17.58
40	3.47	253	–5.39	16.92
50	2.91	273	–5.98	16.34
60	2.36	246	–6.50	15.82
70	1.73	216	–7.07	15.26
80	1.00	183	–7.72	14.60
90	0.19	183	–8.45	13.80
100	–0.53	210	–9.30	12.98
110	–1.14	260	–10.00	12.29
120	–1.57	390	–10.62	11.69
150	–2.32	780	–11.67	10.66
200	–3.06	1200	–12.50	9.86
250	–3.55	1400	–13.10	9.30
300	–4.00	1500	–13.60	8.90

Table 3: FALC model, part 1.

h km	τ_{500}	m g cm^{-2}	T K	v_t km s^{-1}	n_H cm^{-3}	n_p cm^{-3}	n_e cm^{-3}	P_{tot} dyn cm^{-2}	P_{gas}/P_{tot}	ρ g cm^{-3}
2218.20	0.00E+00	6.777E−06	100000	11.73	5.575E+09	5.575E+09	6.665E+09	1.857E−01	0.952	1.31E−14
2216.50	7.70E−10	6.779E−06	95600	11.65	5.838E+09	5.837E+09	6.947E+09	1.857E−01	0.950	1.37E−14
2214.89	1.53E−09	6.781E−06	90816	11.56	6.151E+09	6.150E+09	7.284E+09	1.858E−01	0.948	1.44E−14
2212.77	2.60E−09	6.785E−06	83891	11.42	6.668E+09	6.667E+09	7.834E+09	1.859E−01	0.945	1.56E−14
2210.64	3.75E−09	6.788E−06	75934	11.25	7.381E+09	7.378E+09	8.576E+09	1.860E−01	0.941	1.73E−14
2209.57	4.38E−09	6.790E−06	71336	11.14	7.864E+09	7.858E+09	9.076E+09	1.860E−01	0.938	1.84E−14
2208.48	5.06E−09	6.792E−06	66145	11.02	8.488E+09	8.476E+09	9.718E+09	1.861E−01	0.935	1.99E−14
2207.38	5.81E−09	6.794E−06	60170	10.86	9.334E+09	9.307E+09	1.059E+10	1.862E−01	0.931	2.19E−14
2206.27	6.64E−09	6.797E−06	53284	10.67	1.053E+10	1.047E+10	1.182E+10	1.862E−01	0.925	2.47E−14
2205.72	7.10E−09	6.798E−06	49385	10.55	1.135E+10	1.125E+10	1.266E+10	1.863E−01	0.921	2.66E−14
2205.21	7.55E−09	6.800E−06	45416	10.42	1.233E+10	1.217E+10	1.365E+10	1.863E−01	0.916	2.89E−14
2204.69	8.05E−09	6.801E−06	41178	10.27	1.356E+10	1.332E+10	1.491E+10	1.863E−01	0.910	3.18E−14
2204.17	8.61E−09	6.803E−06	36594	10.09	1.521E+10	1.483E+10	1.657E+10	1.864E−01	0.903	3.56E−14
2203.68	9.19E−09	6.805E−06	32145	9.90	1.724E+10	1.667E+10	1.858E+10	1.864E−01	0.894	4.04E−14
2203.21	9.81E−09	6.807E−06	27972	9.70	1.971E+10	1.887E+10	2.098E+10	1.865E−01	0.883	4.62E−14
2202.75	1.05E−08	6.809E−06	24056	9.51	2.276E+10	2.154E+10	2.389E+10	1.866E−01	0.871	5.33E−14
2202.27	1.13E−08	6.812E−06	20416	9.30	2.658E+10	2.483E+10	2.743E+10	1.866E−01	0.856	6.23E−14
2201.87	1.21E−08	6.815E−06	17925	9.13	3.008E+10	2.778E+10	3.049E+10	1.867E−01	0.843	7.05E−14
2201.60	1.27E−08	6.817E−06	16500	9.02	3.255E+10	2.979E+10	3.256E+10	1.868E−01	0.834	7.63E−14
2201.19	1.36E−08	6.820E−06	15000	8.90	3.570E+10	3.218E+10	3.498E+10	1.869E−01	0.823	8.36E−14
2200.85	1.44E−08	6.823E−06	14250	8.83	3.762E+10	3.343E+10	3.619E+10	1.869E−01	0.816	8.81E−14
2200.10	1.63E−08	6.830E−06	13500	8.74	4.013E+10	3.441E+10	3.699E+10	1.871E−01	0.808	9.40E−14
2199.00	1.90E−08	6.840E−06	13000	8.66	4.244E+10	3.456E+10	3.695E+10	1.874E−01	0.801	9.94E−14
2190.00	4.15E−08	6.936E−06	12000	8.48	4.854E+10	3.411E+10	3.663E+10	1.900E−01	0.785	1.14E−13
2168.00	9.85E−08	7.203E−06	11150	8.30	5.500E+10	3.619E+10	3.889E+10	1.974E−01	0.775	1.29E−13
2140.00	1.76E−07	7.588E−06	10550	8.10	6.252E+10	3.806E+10	4.095E+10	2.079E−01	0.769	1.46E−13
2110.00	2.62E−07	8.063E−06	9900	7.87	7.314E+10	3.923E+10	4.238E+10	2.209E−01	0.760	1.71E−13
2087.00	3.30E−07	8.483E−06	9450	7.70	8.287E+10	3.954E+10	4.291E+10	2.324E−01	0.753	1.94E−13
2075.00	3.66E−07	8.724E−06	9200	7.61	8.882E+10	3.956E+10	4.305E+10	2.390E−01	0.748	2.08E−13
2062.00	4.05E−07	9.005E−06	8950	7.52	9.569E+10	3.952E+10	4.314E+10	2.467E−01	0.743	2.24E−13
2043.00	4.62E−07	9.453E−06	8700	7.41	1.055E+11	3.937E+10	4.314E+10	2.590E−01	0.738	2.47E−13
2017.00	5.41E−07	1.014E−05	8400	7.26	1.203E+11	3.921E+10	4.313E+10	2.778E−01	0.732	2.82E−13
1980.00	6.53E−07	1.128E−05	8050	7.06	1.446E+11	3.908E+10	4.310E+10	3.092E−01	0.727	3.39E−13
1915.00	8.53E−07	1.387E−05	7650	6.74	1.971E+11	3.974E+10	4.351E+10	3.800E−01	0.724	4.62E−13
1860.00	1.03E−06	1.676E−05	7450	6.49	2.547E+11	4.100E+10	4.423E+10	4.593E−01	0.727	5.97E−13
1775.00	1.31E−06	2.298E−05	7250	6.12	3.788E+11	4.399E+10	4.630E+10	6.297E−01	0.736	8.87E−13
1670.00	1.69E−06	3.510E−05	7050	5.69	6.292E+11	4.922E+10	5.085E+10	9.616E−01	0.752	1.47E−12
1580.00	2.07E−06	5.186E−05	6900	5.34	9.900E+11	5.390E+10	5.535E+10	1.421E+00	0.767	2.32E−12
1475.00	2.59E−06	8.435E−05	6720	4.93	1.726E+12	6.037E+10	6.191E+10	2.311E+00	0.787	4.05E−12
1378.00	3.19E−06	1.363E−04	6560	4.53	2.970E+12	6.824E+10	7.007E+10	3.735E+00	0.809	6.96E−12

Table 4: FALC model, part 2.

h km	τ_{500}	m g cm^{-2}	T K	v_t km s^{-1}	n_H cm^{-3}	n_p cm^{-3}	n_e cm^{-3}	P_{tot} dyn cm^{-2}	P_{gas}/P_{tot}	ρ g cm^{-3}
1278.00	4.02E−06	2.312E−04	6390	4.04	5.393E+12	7.768E+10	7.994E+10	6.335E+00	0.837	1.26E−11
1180.00	5.19E−06	4.022E−04	6230	3.53	1.002E+13	8.783E+10	9.083E+10	1.102E+01	0.867	2.35E−11
1065.00	7.43E−06	8.074E−04	6040	2.94	2.164E+13	9.992E+10	1.047E+11	2.212E+01	0.901	5.07E−11
980.00	1.03E−05	1.396E−03	5900	2.52	3.931E+13	1.068E+11	1.142E+11	3.824E+01	0.924	9.21E−11
905.00	1.44E−05	2.314E−03	5755	2.19	6.806E+13	1.078E+11	1.192E+11	6.341E+01	0.940	1.59E−10
855.00	1.85E−05	3.282E−03	5650	1.99	9.931E+13	1.051E+11	1.208E+11	8.993E+01	0.949	2.33E−10
805.00	2.39E−05	4.710E−03	5490	1.77	1.481E+14	9.014E+10	1.122E+11	1.290E+02	0.958	3.47E−10
755.00	3.09E−05	6.868E−03	5280	1.54	2.268E+14	6.493E+10	9.690E+10	1.882E+02	0.967	5.31E−10
705.00	4.00E−05	1.022E−02	5030	1.38	3.560E+14	3.637E+10	8.387E+10	2.799E+02	0.972	8.34E−10
650.00	5.55E−05	1.624E−02	4750	1.18	6.033E+14	1.375E+10	9.000E+10	4.451E+02	0.978	1.41E−09
600.00	8.53E−05	2.538E−02	4550	1.00	9.895E+14	5.368E+09	1.255E+11	6.954E+02	0.983	2.32E−09
560.00	1.40E−04	3.680E−02	4430	0.89	1.478E+15	2.825E+09	1.767E+11	1.008E+03	0.986	3.46E−09
525.00	2.39E−04	5.125E−02	4400	0.80	2.078E+15	2.424E+09	2.413E+11	1.404E+03	0.989	4.87E−09
490.00	4.29E−04	7.149E−02	4410	0.72	2.898E+15	2.618E+09	3.300E+11	1.959E+03	0.991	6.79E−09
450.00	8.51E−04	1.044E−01	4460	0.65	4.192E+15	3.600E+09	4.714E+11	2.860E+03	0.993	9.82E−09
400.00	1.98E−03	1.664E−01	4560	0.55	6.549E+15	6.715E+09	7.344E+11	4.558E+03	0.995	1.53E−08
350.00	4.53E−03	2.626E−01	4660	0.52	1.012E+16	1.267E+10	1.134E+12	7.194E+03	0.996	2.37E−08
300.00	1.01E−02	4.103E−01	4770	0.55	1.545E+16	2.604E+10	1.737E+12	1.124E+04	0.995	3.62E−08
250.00	2.20E−02	6.344E−01	4880	0.63	2.331E+16	5.605E+10	2.645E+12	1.738E+04	0.994	5.46E−08
200.00	4.73E−02	9.705E−01	4990	0.79	3.476E+16	1.253E+11	4.004E+12	2.659E+04	0.990	8.14E−08
175.00	6.87E−02	1.195E+00	5060	0.90	4.211E+16	2.028E+11	4.945E+12	3.274E+04	0.988	9.87E−08
150.00	9.92E−02	1.466E+00	5150	1.00	5.062E+16	3.579E+11	6.153E+12	4.017E+04	0.985	1.19E−07
125.00	1.42E−01	1.790E+00	5270	1.10	6.024E+16	7.119E+11	7.770E+12	4.905E+04	0.983	1.41E−07
100.00	2.02E−01	2.174E+00	5410	1.20	7.107E+16	1.485E+12	1.003E+13	5.957E+04	0.980	1.67E−07
75.00	2.87E−01	2.625E+00	5580	1.30	8.295E+16	3.281E+12	1.353E+13	7.192E+04	0.977	1.94E−07
50.00	4.13E−01	3.148E+00	5790	1.40	9.558E+16	7.614E+12	1.980E+13	8.624E+04	0.975	2.24E−07
35.00	5.22E−01	3.496E+00	5980	1.46	1.027E+17	1.439E+13	2.779E+13	9.578E+04	0.973	2.40E−07
20.00	6.75E−01	3.869E+00	6180	1.52	1.098E+17	2.588E+13	4.064E+13	1.060E+05	0.972	2.57E−07
10.00	8.14E−01	4.132E+00	6340	1.55	1.142E+17	3.926E+13	5.501E+13	1.132E+05	0.971	2.68E−07
0.00	1.00E+00	4.404E+00	6520	1.60	1.182E+17	6.014E+13	7.697E+13	1.207E+05	0.971	2.77E−07
−10.00	1.25E+00	4.686E+00	6720	1.64	1.219E+17	9.269E+13	1.107E+14	1.284E+05	0.970	2.86E-07
−20.00	1.61E+00	4.975E+00	6980	1.67	1.246E+17	1.536E+14	1.730E+14	1.363E+05	0.970	2.92E-07
−30.00	2.14E+00	5.269E+00	7280	1.70	1.264E+17	2.597E+14	2.807E+14	1.444E+05	0.970	2.96E-07
−40.00	2.95E+00	5.567E+00	7590	1.73	1.280E+17	4.249E+14	4.480E+14	1.525E+05	0.971	3.00E-07
−50.00	4.13E+00	5.869E+00	7900	1.75	1.295E+17	6.668E+14	6.923E+14	1.608E+05	0.971	3.04E-07
−60.00	5.86E+00	6.174E+00	8220	1.77	1.307E+17	1.022E+15	1.050E+15	1.691E+05	0.972	3.06E-07
−70.00	8.36E+00	6.481E+00	8540	1.79	1.317E+17	1.515E+15	1.546E+15	1.776E+05	0.972	3.09E-07
−80.00	1.20E+01	6.790E+00	8860	1.80	1.325E+17	2.180E+15	2.215E+15	1.860E+05	0.973	3.10E-07
−90.00	1.70E+01	7.102E+00	9140	1.82	1.337E+17	2.942E+15	2.979E+15	1.946E+05	0.973	3.13E-07
−100.00	2.36E+01	7.417E+00	9400	1.83	1.351E+17	3.826E+15	3.867E+15	2.032E+05	0.974	3.17E-07

2   Continuous spectrum from the solar atmosphere

We now turn to the formation of the solar continuum radiation, concentrating on the visible and near-infrared parts of its spectrum.

Figure 4:   Subrahmanyan Chandrasekhar (1910–1995) is regarded by many as the greatest astronomer of the twentieth century. He also played an important role in the topic of this exercise, undertaking a very lengthy and difficult calculation (not a computation, no computers yet at that time!) of the bound-free and free-free extinction cross-sections of the H⁻ ion, together with F.H. Breen. Their result, published in Chandrasekhar & Breen (1946) will be duplicated in one of your graphs below. The shape of the extinction curve, with a peak near $\lambda = 10000$ Å and a minimum at the H⁻ bound-free ionization limit at $\lambda = 16000$ Å, reproduced the observed spectral variation of the unknown solar continuum extinction as derived already by G.F.W. Mulders at Utrecht in 1935 for $\lambda = 4000 - 25000$ Å. The brilliant suggestion that H⁻ might cause this extinction, instead of the ensemble of unknown metal edges that was earlier postulated, had already been given by Pannekoek (1930) (on page 166) but was forgotten until it came independently from Wildt (1939). The proof came with Chandrasekhar's laborious quantummechanical evaluation and explained how the solar atmosphere can be opaque at gas densities much lower than the transparent air around us, as you found in the previous exercise. It revolutionized the understanding of cool-star atmospheres by much increasing their hydrogen-to-metals ratio and gas pressure compared with the earlier metallic-absorption modeling of Biermann, Unsöld and Pannekoek himself. A more detailed description is found in Hearnshaw (1986). Picture copied from the "Astronomy Picture of the Day" website (`http://apod.nasa.gov/apod`).

2.1   Observed solar continua

Table 5 specifies the continuum radiation emitted by the sun in the wavelength range $\lambda = 0.2 - 5\ \mu$m, taken from Allen (1976). The table caption defines four different quantities as a function of wavelength, respectively the radially emergent intensity and the astrophysical flux in the solar continuum with and without smoothed lines. The units are cgs with $\Delta\lambda = 1\ \mu$m for the spectral bandwidth. The table is available as file `solspect.dat` at `http:/www.staff.science.uu.nl/˜rutte101/rrweb/rjr-edu/exercises/ssb/`.

- Write IDL code to read Table 5.

- Plot the four spectral distributions together in one figure over the range $\lambda = 0 - 2\ \mu$m. Use a statement such as
    ```
    print,' max(Ic) =',max(Icont), ' at ',wav[where(Icont eq max(Icont))]
    ```
    to check that the continuum intensity reaches $I_\lambda^c = 4.6 \times 10^{10}$ erg cm^{-2} s^{-1} ster^{-1} μm^{-1} at $\lambda = 0.41\ \mu$m. Explain why the four distributions share the same units and discuss the differences between them.

11

- Convert these spectral distributions into values per frequency bandwidth $\Delta \nu = 1$ Hz. Plot these also against wavelength. Check: peak $I_\nu^c = 4.21 \times 10^{-5}$ erg cm^{-2} s^{-1} ster^{-1} Hz^{-1} at $\lambda = 0.80\,\mu$m.

- Write an IDL function `planck.pro` (or use your routine from Exercises *"Stellar Spectra A: Basic Line Formation"*, or use mine) that computes the Planck function in the same units. Try to fit a Planck function to the solar continuum intensity. What rough temperature estimate do you get?

- Invert the Planck function analytically to obtain an equation which converts an intensity distribution I_λ into brightness temperature T_b (defined by $B_\lambda(T_b) \equiv I_\lambda$). Code it as an IDL function and use that to plot the brightness temperature of the solar continuum against wavelength (with the `plot,/ynozero` keyword). Discuss the shape of this curve. It peaks near $\lambda = 1.6\,\mu$m. What does that mean for the radiation escape at this wavelength?
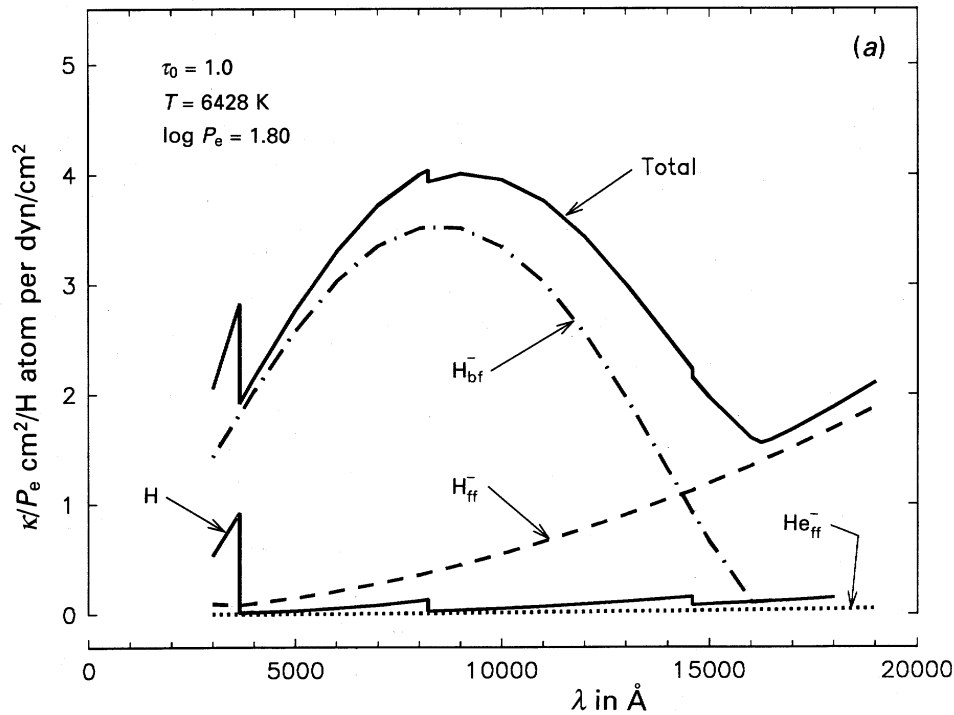

Figure 5: Continuous extinction coefficients κ_ν^c for hydrogen and helium, per neutral hydrogen atom and per unit electron pressure, for the depth $\tau_0 = 1$ (continuum optical depth at $\lambda = 500$ nm) in the photosphere of a solar-like dwarf star. The coefficients κ are here measured per neutral hydrogen atom in whatever state of excitation, assuming Saha-Boltzmann population partitioning, and normalized by the electron pressure $P_e = n_e k T$. The cross-sections are in units of 10^{-26} cm^2 (not cm^2 as specified in the y-axis label); stimulated emission was not included in the computation of these curves. The H^- curve shows the bound-free Balmer, Paschen and Brackett edges, plus part of the Pfund edge at right. The curves do not extend beyond the Balmer edge at left where the neglected metal edges become important. Thomson scattering is also neglected. From page 140 of Gray (1992).

2.2 Continuous extinction

We will assume that H$^-$ (a hydrogen atom with an extra electron) is the major provider of continuous extinction in the solar atmosphere. This is quite a good assumption for the solar photosphere for wavelengths $\lambda > 0.5\,\mu$m (5000 Å). The second-best extinction provider are H I bound-free interactions, at only a few percent. This may be seen in Figure 5 taken from Gray (1992).
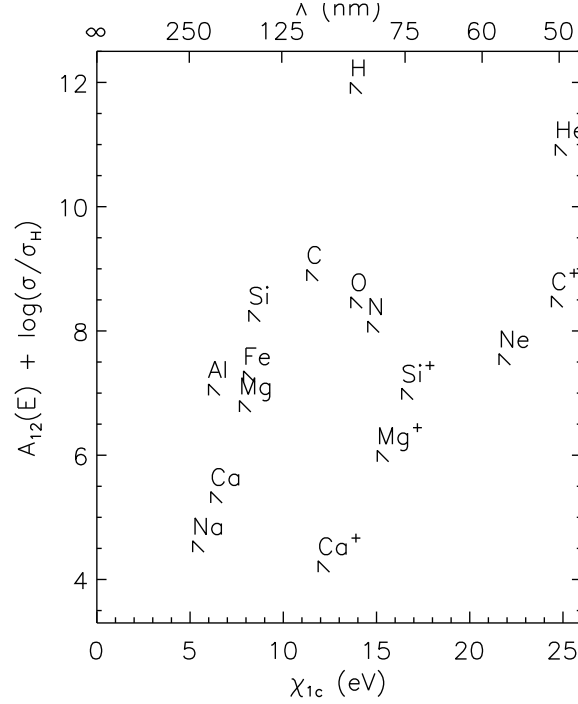
12

Figure 6: Ionization edges for a selection of abundant elements. The triangular symbols depict bound-free continuum edges in the form of schematic hydrogenic ν^{-3} decay functions above each ionization threshold. The plot shows the edge distribution over ionization energy χ_{1c} (along the bottom) or threshold wavelength (along the top) and the logarithmic product of the element abundance $A_{12} \equiv \log(n_E/n_H + 12)$ and the bound-free cross-section per particle at threshold σ/σ_H (vertically). Thus, it shows the relative importance of the major bound-free edges throughout the spectrum. They are all at ultraviolet wavelengths and do not contribute extinction in the visible and infrared. The plus signs indicate important first-ion edges; higher ionization stages produce edges at yet shorter wavelengths. The abundance values come from Engvold (1977), the ionization energies from Novotny (1973), the cross-sections from the chapter by Baschek and Scholtz in Aller et al. (1982). Thijs Krijger production following unpublished lecture notes by E.H. Avrett, taken from my RTSA lecture notes available at `http://www.staff.science.uu.nl/~rutte101/Course_notes.html`.

Below $\lambda = 500$ nm there is heavy line crowding (not added in Figure 5) which acts as a quasi-continuum. Below $\lambda = 365$ nm the Balmer bound-free edge provides large extinction, and at yet shorter wavelengths the bound-free ionizaton edges of various metals (Al I, Mg I, Fe I, Si I, C I) provide steep extinction increase yet before the H I Lyman continuum sets is, as may be expected from Figure 6. In this exercise we will neglect these contributions by evaluating only the H$^-$ extinction and the extinction due to scattering off free electrons (Thomson scattering).

IDL function `exthmin.pro` evaluates polynomial fits for H$^-$ extinction that are given on page 135 ff of Gray (1992). The routine delivers the total (bound-free plus free-free) H$^-$ extinction in units of cm^2 per neutral hydrogen atom (*not* per H$^-$ ion!). LTE is assumed in the computation of the H$^-$ ion density relative to the neutral hydrogen density (through a Saha equation where the neutral atom takes the place of the ionized state, see page 135 of Gray (1992).

- Pull `exthmin.pro` over and compare it to Gray's formulation.

- Plot the wavelength variation of the H$^-$ extinction for the FALC parameters at $h = 0$ km (see Tables 3–4). This plot reproduces the result of Chandrasekhar & Breen (1946). Compare it to Gray's version

in Figure 5.

- Hydrogenic bound-free edges behave just as H I with maximum extinction at the ionization limit and decay $\sim \lambda^3$ for smaller wavelengths, as indeed shown by the H I curve in Figure 5. The H$^-$ bound-free extinction differs strongly from this pattern. Why is it not hydrogenic although due to hydrogen?

- How should you plot this variation to make it look like the solar brightness temperature variation with wavelength? Why?

- Read in the FALC model atmosphere (see the previous exercise). Note that column n_H in the FALC model of Tables 3–4 is the total hydrogen density, summing neutral atoms and free protons (and H_2 molecules but those are virtually absent). This is seen by inspecting the values of n_H and n_p at the top of the FALC table where all hydrogen is ionised. Gray's H$^-$ extinction is measured per neutral hydrogen atom, so you have to multiply the height-dependent result from `exthmin(wav,temp,eldens)` with $n_{\mathrm{neutral\,H}} \approx n_H(h) - n_p(h)$ to obtain extinction $\alpha_\lambda(H^-)$ measured per cm path length (or cross-section per cubic cm) at every height h. Plot the variation of the H$^-$ extinction per cm with height for $\lambda = 0.5\,\mu$m. This plot needs to be logarithmic in y, why?

- Now add the Thomson scattering off free electrons to the extinction per cm. The Thomson cross-section per electron is the same at all wavelengths and is given by

$$\sigma^T = 6.648 \times 10^{-25} \ \mathrm{cm}^2. \tag{5}$$

With which height-dependent quantity do you have to multiply this number to obtain extinction per cm? Overplot this contribution to the continuous extinction $\alpha_\lambda^c(h)$ in your graph and then overplot the total continuous extinction too. Explain the result.

2.3 Optical depth

Knowing the stratification (FALC model) and the continuous extinction as function of height, we may now compute the corresponding optical depth scale given by:

$$\tau_\lambda(h_0) \equiv - \int_\infty^{h_0} \alpha_\lambda^c \, \mathrm{d}h \tag{6}$$

at any height h_0. Note that FALC is tabulated in reverse order, corresponding to the $-h$ direction. The IDL library routine INT_TABULATED supplies a closed five-point Newton-Cotes integration routine that might be applied, but the simple trapezium rule gives nearly identical results. (It is often much safer to use trapezoidal integration than higher-order schemes. The latter may give wildly wrong answers by fitting the samples with large excursions in between samples. A good recipe is to always stick to trapezoidal integration and to refine the grid if higher precision is desired.)

- Integrate the extinction at $\lambda = 500$ nm to obtain the τ_{500} scale and compare it graphically to the FALC τ_{500} scale. Here is my code, with `ext(ih)` denoting the continuous extinction per cm at $\lambda = 500$ nm and at height `h(ih)`:

```
; compute and plot tau at 500 nm, compare with FALC tau5
tau=fltarr(nh)
for ih=1,nh-1 do tau[ih]=tau[ih-1]+$
   0.5*(ext[ih]+ext[ih-1])*(h[ih-1]-h[ih])*1E5
plot,h,tau,/ylog,$
  xtitle='height [km]',ytitle='tau at 500 nm'
oplot,h,tau5,linestyle=2
```

14

2.4 Emergent intensity and height of formation

We are now ready to compute the intensity of the radiation that emerges from the center of the solar disk (in the radial direction from the solar sphere). It is given (assuming plane-parallel stratification) by:

$$I_\lambda = \int_0^\infty S_\lambda \, e^{-\tau_\lambda} \, d\tau_\lambda. \tag{7}$$

It is interesting to also inspect the intensity contribution function

$$\frac{dI_\lambda}{dh} = S_\lambda \, e^{-\tau_\lambda} \alpha_\lambda \tag{8}$$

which shows the contribution of each layer to the emergent intensity. Its weighted mean defines the "mean height of formation":

$$<h> \equiv \frac{\int_0^\infty h \, (dI_\lambda/dh) \, dh}{\int_0^\infty (dI_\lambda/dh) \, dh} = \frac{\int_0^\infty h \, S_\lambda \, e^{-\tau_\lambda} \, d\tau_\lambda}{\int_0^\infty S_\lambda \, e^{-\tau_\lambda} \, d\tau_\lambda}. \tag{9}$$

Here is my code to compute and diagnose these quantities for a given wavelength (wl in μm) assuming LTE and using trapezoidal integration:

```
; emergent intensity at wavelength wl (micron)
ext=fltarr(nh)
tau=fltarr(nh)
integrand=fltarr(nh)
contfunc=fltarr(nh)
int=0.
hint=0.
for ih=1,nh-1 do begin
  ext[ih]=exthmin(wl*1E4,temp[ih],nel[ih])*(nhyd[ih]-nprot[ih])$
          +0.664E-24*nel[ih]
  tau[ih]=tau[ih-1]+0.5*(ext[ih]+ext[ih-1])*(h[ih-1]-h[ih])*1E5
  integrand[ih]=planck(temp[ih],wl)*exp(-tau[ih])
  int=int+0.5*(integrand[ih]+integrand[ih-1])*(tau[ih]-tau[ih-1])
  hint=hint+h[ih]*0.5*(integrand[ih]+integrand[ih-1])*(tau[ih]-tau[ih-1])
  contfunc[ih]=integrand[ih]*ext[ih]
endfor
hmean=hint/int
```

- The code above sits in file emergint.pro. Copy it into your IDL program and make it work setting wl=0.5.

- Compare the computed intensity at $\lambda = 500$ nm with the observed intensity, using a statement such as
```
print,' observed cont int = ',Icont[where(wl eq wav)]
```
  to obtain the latter.

- Plot the peak-normalized contribution function against height and compare its peak location with the mean height of formation.

- Repeat the above for $\lambda = 1 \, \mu$m, $\lambda = 1.6 \, \mu$m, and $\lambda = 5 \, \mu$m. Discuss the changes of the contribution functions and their cause.

- Check the validity of the LTE Eddington-Barbier approximation $I_\lambda \approx B_\lambda(T[\tau_\lambda = 1])$ by comparing the mean heights of formation with the $\tau_\lambda = 1$ locations and with the locations where $T_b = T(h)$.

2.5 Disk-center intensity

The solar disk-center intensity spectrum can now be computed by repeating the above in a big loop over wavelength.

- Compute the emergent continuum over the wavelength range of Table 5.

- Compare it graphically with the observed solar continuum in Table 5 and file `solspect.dat`.

2.6 Limb darkening

The code is easily modified to give the intensity that emerges under an angle $\mu = \cos\theta$, in plane-parallel approximation given by:

$$I_\lambda(0,\mu) = \int_0^\infty S_\lambda \, e^{-\tau_\lambda/\mu} \, d\tau_\lambda/\mu. \tag{10}$$

- Repeat the intensity evaluation using (10) within an outer loop over $\mu = 0.1, 0.2, \ldots, 1.0$.

- Plot the computed ratio $I_\lambda(0,\mu)/I_\lambda(0,1)$ at a few selected wavelengths, against μ and also against the radius of the apparent solar disk $r/R_\odot = \sin\theta$. Explain the limb darkening and its variation with wavelength.

2.7 Flux integration

The emergent intensity may now be integrated over emergence angle to get the emergent astrophysical flux:

$$F_\lambda(0) = 2\int_0^1 I_\lambda(0,\mu)\,\mu\,d\mu. \tag{11}$$

The problem arises that (10) cannot be evaluated at $\mu = 0$. The naive way to get F is simply to integrate $I_\lambda(0,\mu)$ trapezoidally over the ten angles $\mu = 0.1, 0.2, \ldots, 1.0$ at which you have it already, but that produces too much flux, even while ignoring the small contribution from the outer limb ($\mu = 0.0 - 0.1$, $\sin\theta = 0.995 - 1.0$), because $I_\lambda(0,\mu)\,\mu$ is a concave function ill-fitted with straight segments. This integral is therefore better evaluated with "open quadrature", an integration formula neglecting the endpoints. Classical equal-spacing recipes are the Open Newton-Cotes quadrature formulae but it is much better to use non-equidistant Gaussian quadrature (see the chapter "Integration of functions" in *Numerical Recipes* by Press et al. (1986).

The defining formula is:

$$\int_{-1}^{+1} f(x)\,dx \approx \sum_{i=1}^n w_i \, f(x_i) \tag{12}$$

and the required abscissa values x_i and weights w_i are tabulated for $n = 2 - 10$ and even higher orders on page 916 of Abramowitz & Stegun (1965). Three-point Gaussian integration is sufficiently accurate for the emergent flux integration.

- Compute the emergent solar flux and compare it to the observed flux in Table 5 and file `solspect.dat`. Here is my code (file `gaussflux.pro`):

16

```
; ===== three-point Gaussian integration intensity -> flux
; abscissae + weights n=3 Abramowitz & Stegun page 916
xgauss=[-0.7745966692,0.0000000000,0.7745966692]
wgauss=[ 0.5555555555,0.8888888888,0.5555555555]
fluxspec=fltarr(nwav)
intmu=fltarr(3,nwav)
for imu=0,2 do begin
  mu=0.5+xgauss[imu]/2.    ; rescale xrange [-1,+1] to [0,1]
  wg=wgauss[imu]/2.        ; weights add up to 2 on [-1,+1]
  for iw=0,nwav-1 do begin
    wl=wav[iw]
    @emergintmu.pro         ; old trapezoidal integration I(0,mu)
    intmu[imu,iw]=int
    fluxspec[iw]=fluxspec[iw]+wg*intmu[imu,iw]*mu
  endfor
endfor
fluxspec=2*fluxspec    ; no !pi, AQ has flux F, not {\cal F}
plot,wav,fluxspec,$
  xrange=[0,2],yrange=[0,5E10],$
  xtitle='wavelength [micron]',ytitle='solar flux'
oplot,wav,Fcont,linestyle=2
xyouts,0.5,4E10,'computed'
xyouts,0.35,1E10,'observed'
```

2.8 Discussion

You have succeeded in explaining the solar continuum at visible and infrared wavelengths as largely due to H$^-$ extinction. This is what Chandrasekhar & Breen (1946) accomplished. The bound-free contribution from H I is small since the required populations of $n = 3$ (Paschen continuum) and $n = 4$ (Brackett continuum) are small (Boltzmann partitioning; cf. Figure 5). Other elements do not contribute continuous extinction in the visible and infrared because their major bound-free edges are all in the ultraviolet (Figure 6).

The large opacity of the solar photosphere is therefore due to the combination of abundant neutral hydrogen atoms, the presence of free electrons (that come mostly from other particle species with lower ionization energy), and the large polarization of the simple electron-proton combination which produces a large cross-section for Coulomb interactions between hydrogen atoms and free electrons. There are no free electrons in our own atmosphere and the molecules making up the air around us possess much better Coulomb shielding; terrestrial air is therefore far less opaque at visible wavelengths than the solar gas. In the infrared, air is similarly transparant in some spectral windows correspondig to energy bands in which the molecules can't rotate or vibrate.

In general, radiative transfer in stellar atmospheres is a difficult subject because in our daily physical experience, gases ought to be transparent. Even though stars are fully gaseous, they are far from transparent. H$^-$ extinction makes even the atmospheres of cool stars less transparent than what we would expect for gases so tenuous.

A final note: while LTE is an excellent assumption for H$^-$ bound-free processes and exactly valid (as long as the Maxwell distribution holds) for H$^-$ free-free processes, it is not at all valid for Thomson scattering. The process source function for purely coherent (monochromatic) scattering is not given by

$B_\lambda(T)$ but by the angle-averaged intensity $J_\lambda \equiv (1/4\pi) \int I_\lambda \, d\Omega$. Obtaining J_λ from such an integration requires knowledge of the intensity $I_\lambda(h, \theta)$ locally and in all directions θ, not just the emergent one at $\tau = 0$ computed here. This evaluation will be treated extensively in exercises *"Stellar Spectra C: NLTE Line Formation"*. For now, such sophistication is too much work, and in any case Thomson scattering is not important for the formation of the solar continuum intensity in this wavelength range (as you can see by deleting or doubling its contribution in your code). However, Thomson scattering dominates the continuous extinction in the photospheres of hot stars in which hydrogen is largely ionized so that the H^- contribution vanishes while the electron contribution rises.

Table 5: *Solar spectral distribution, from Allen (1976). F_λ = astrophysical flux at the solar surface with spectral irregularities smoothed; F'_λ = astrophysical flux at the solar surface for the continuum between lines; I_λ = radially emergent intensity at the solar surface with spectral irregularities smoothed; I'_λ = radially emergent intensity at the solar surface for the continuum between lines. "Astrophysical" flux F_λ is defined as $\pi F_\lambda \equiv \mathcal{F}_\lambda$ with $\mathcal{F}_\lambda$ the net outward flow of energy through a stellar surface element. The astrophysical flux is often prefered because it has $F_\lambda = <I_\lambda>$ with $<I_\lambda>$ the intensity averaged over the stellar disk received by a distant observer. It has the same dimension as intensity, whereas $\mathcal{F}_\lambda$ is not measured per steradian.*

λ μm	F_λ	F'_λ 10^{10} erg cm^{-2} s^{-1} μm^{-1} ster^{-1}	I_λ	I'_λ
0.20	0.02	0.04	0.03	0.04
0.22	0.07	0.11	0.14	0.20
0.24	0.09	0.2	0.18	0.30
0.26	0.19	0.4	0.37	0.5
0.28	0.35	0.7	0.59	1.19
0.30	0.76	1.36	1.21	2.15
0.32	1.10	1.90	1.61	2.83
0.34	1.33	2.11	1.91	3.01
0.36	1.46	2.30	2.03	3.20
0.37	1.57	2.50	2.33	3.62
0.38	1.46	2.85	2.14	4.1
0.39	1.53	3.10	2.20	4.4
0.40	2.05	3.25	2.9	4.58
0.41	2.46	3.30	3.43	4.60
0.42	2.47	3.35	3.42	4.59
0.43	2.46	3.36	3.35	4.55
0.44	2.66	3.38	3.58	4.54
0.45	2.90	3.40	3.86	4.48
0.46	2.93	3.35	3.88	4.40
0.48	2.86	3.30	3.73	4.31
0.50	2.83	3.19	3.63	4.08
0.55	2.72	2.94	3.40	3.68
0.60	2.58	2.67	3.16	3.27
0.65	2.31	2.42	2.78	2.88
0.70	2.10	2.13	2.50	2.53
0.75	1.88	1.91	2.22	2.24
0.8	1.69	1.70	1.96	1.97
0.9	1.33	1.36	1.53	1.55
1.0	1.08	1.09	1.21	1.23
1.2	0.73	0.74	0.81	0.81
1.4	0.512	0.512	0.564	0.564
1.6	0.375	0.375	0.403	0.403
1.8	0.248	0.248	0.268	0.268
2.0	0.171	0.171	0.183	0.183
2.5	0.0756	0.0756	0.081	0.081
3.0	0.0386	0.0386	0.041	0.041
4.0	0.0130	0.0130	0.0135	0.0135
5.0	0.0055	0.0055	0.0057	0.0057

3   Spectral lines from the solar atmosphere

We now turn to the formation of spectral lines in the solar spectrum. We will concentrate on the formation of the Na I D_1 line at $\lambda = 589.6$ nm.

Figure 7: Albrecht O.J. Unsöld (1905 – 1995) was the first, in 1941 at Kiel, to study stellar composition ("abundance analysis") in the detail permitted by proper physical understanding of line formation (for the B0 dwarf τ Scorpii, using spectrograms taken during a six-month visit to the US just before the second world war). He used the so-called "coarse" analysis based on Minnaert's curve of growth for a Schuster-Schwarzschild single "reversing layer" as in the third exercise of "Stellar Spectra A: Basic Line Formation". Later, he led a school of astrophysicists at Kiel in "fine analysis", combining LTE line formation with non-grey stratified atmosphere modeling just as you do in this exercise. The technique was developed by L.H. Aller, C. de Jager and others in the fifties, and has dominated stellar abundance analysis throughout the second half of the twentieth century. He spelled out its physical basis in great detail in his "Physik der Sternatmosphären" (Unsöld 1955). Portrait copied from Hearnshaw (1986)

3.1   Observed Na D line profiles

The solar Na I D lines are shown in Figure 8.

- Pull the data that went into making Figure 8 over from `ftp://vso.nso.edu/pub/atlas/visatl`. Concatenate the files covering the two Na I D lines (sp16900 and sp16950) into a single file, deleting the overlaps.

- Write IDL code to read these data. You need the first and third columns (see the README).

3.2   Na D wavelengths

The README suggests that the first column specifies frequencies, but these numbers are actually wavenumbers $\sigma = 1/\lambda_{\mathrm{vac}}$ in cm^{-1}. If you invert them into wavelengths they differ by a few Ångstrom (in this wavelength region) from the standard-air wavelengths λ_{air} habitually used for spectral lines with $\lambda > 2000$ Å.

- Plot the solar Na I D lines against vacuum wavelength at various dispersions.

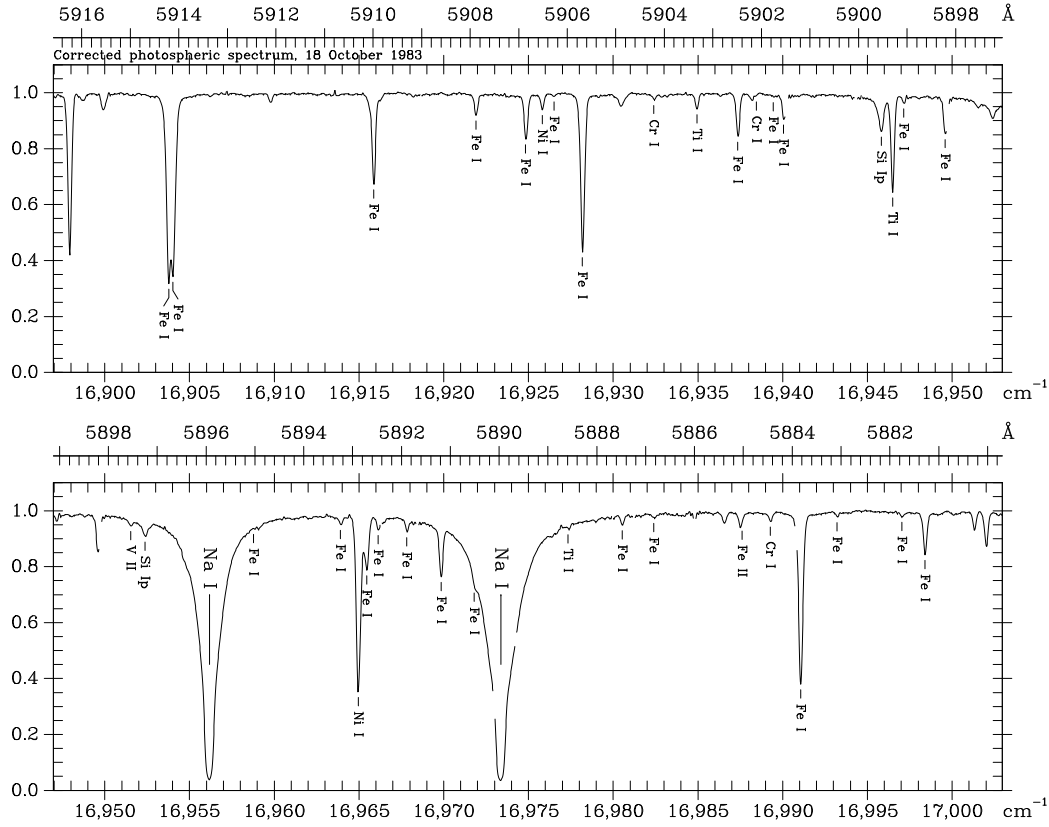- Find the vacuum wavelengths of their minima (use the IDL `where` and `min` functions).

Figure 8: A page out of the solar disk-center intensity atlas of Wallace et al. (1998). The intensity scale (vertical) is in relative units, normalized to the local continuum intensity between the lines. The lower horizontal scales specify wavenumbers in cm^{-1}, the upper ones vacuum wavelengths in Å. The Na I D_1 line is the one to the left because Fraunhofer catalogued the solar spectrum features from red to blue. The atlas was made with the Fourier Transform Spectrometer at the McMath-Pierce solar telescope at Kitt Peak (Brault 1980). Telluric lines have been removed. Both the atlas pages and the input data are available at `ftp://vso.nso.edu/pub/atlas/visatl`.

- Check that the Na I D wavelengths tabulated in the solar spectrum line list of Moore et al. (1966) (computer-readable at `ftp://vso.nso.edu/pub/atlas/linelist/Moore`) are $\lambda = 5895.94$ Å for Na I D_1 and $\lambda = 5889.97$ Å for Na I D_2, respectively. Check the identification of a few blends (other lines) in Figure 8 with the entries in this table[2].

- The Astrolib[3] routines `airtovac` and `vactoair` convert air into vacuum wavelengths and vice versa. A reasonably accurate transformation is also given by

$$\lambda_{\mathrm{air}} = 0.99972683\,\lambda_{\mathrm{vac}} + 0.0107 - 196.25/\lambda_{\mathrm{vac}} \tag{13}$$

with both λ's in Å, from Neckel 1999[4]. Use this equation or routine `vactoair` to plot the Na I D lines

---

[2]The solar spectrum line list was constructed at Utrecht. All equivalent widths were measured by hand, hard labour for many during two decades. The line identifications were made from laboratory wavelength tables compiled by Mrs. Charlotte Moore and co-workers at the US National Bureau of Standards.

[3]IDL astrolib at `http://idlastro.gsfc.nasa.gov`

[4]The announcement of two solar atlases, respectively for disk-averaged and disk-center intensity, constructed from the same FTS data from which the similar NSO atlases were made. These also specify calibrated absolute intensities. They are available through anonymous ftp at `ftp://ftp.hs.uni-hamburg.de/pub/outgoing/FTS-Atlas`.

against air wavelength.

3.3   LTE line formation

We will now compute the solar Na I D$_1$ line assuming the FALC model atmosphere and LTE for the line source function. Since LTE holds already for the continuum processes at these wavelengths (being dominated by H$^-$ bound-free transitions), the assumption of LTE line formation implies that you can simply set $S_\lambda^l = S_\lambda^c = S_\lambda^{\text{total}} = B_\lambda(T)$. What remains is first to evaluate the line extinction as a function of height and wavelength, and then to add that to the continuous extinction in the integration loop of the previous exercise. The outer loop over wavelength then has to sample the Na I D1 profile.

3.4   Line extinction

The monochromatic line extinction per cm path lenght for a bound-bound transition between a lower level l and an upper level u is given by:

$$\alpha_\lambda^l = \frac{\sqrt{\pi}e^2}{m_e c} \frac{\lambda^2}{c} b_l \frac{n_l^{\text{LTE}}}{N_E} N_H A_E f_{lu} \frac{H(a,v)}{\Delta\lambda_D} \left[1 - \frac{b_u}{b_l} e^{-hc/\lambda kT}\right], \tag{14}$$

which holds generally when the line broadening is described by the Voigt function $H(a,v)$, a valid assumption for most lines (but hydrogen lines are broadened with the Holtsmark distribution). For LTE the population departure coefficients of the lower and upper levels are $b_l = b_u = 1$. The LTE population fraction n_l^{LTE}/N_E (lower level population scaled by the total element population) is given by the combined Saha and Boltzmann distributions

$$U_r \equiv \sum_s g_{r,s}\, e^{-\chi_{r,s}/kT} \tag{15}$$

$$\frac{n_{r,s}}{N_r} = \frac{g_{r,s}}{U_r}\, e^{-\chi_{r,s}/kT} \tag{16}$$

$$\frac{N_{r+1}}{N_r} = \frac{1}{N_e}\frac{2U_{r+1}}{U_r}\left(\frac{2\pi m_e kT}{h^2}\right)^{3/2} e^{-\chi_r/kT}, \tag{17}$$

where s is the level counter and r the ionization stage counter.

Some numbers for the Na I D$_1$ and Na I D$_2$ lines:

- sodium ionization energies $\chi_1 = 5.139$ eV, $\chi_2 = 47.29$ eV, $\chi_3 = 71.64$ eV (Appendix D of Gray 1992);

- the Na I D$_1$ and Na I D$_2$ lower-level excitation energy $\chi_{1,1} = 0$ eV (shared ground state);

- the Na I D$_1$ and Na I D$_2$ lower-level statistical weight $g_{1,1} = 2$ (ground state 3s 2S$_{1/2}$, $g = 2J+1$). The upper-level statistical weights are 2 and 4 for Na I D$_1$ (3p 2P$_{1/2}^o$) and Na I D$_2$ (3p 2P$_{3/2}^o$), respectively;

- the oscillator strengths are $f_{lu} = 0.318$ for Na I D$_1$, $f_{lu} = 0.631$ for Na I D$_2$;

- the Na I partition function defined by (15) is given in Appendix D of Gray (1992) as $\log U_{\text{Na I}}(T) \approx c_0 + c_1 \log\theta + c_2 \log^2\theta + c_3 \log^3\theta + c_4 \log^4\theta$ with $\theta \equiv 5040./T$ and $c_0 = 0.30955$, $c_1 = -0.17778$, $c_2 = 1.10594$, $c_3 = -2.42847$ and $c_4 = 1.70721$. In the next edition (Gray 2005) these polynomial fits were replaced by a $\log U$ table;

- the Na II and Na III partition functions are well approximated by the statistical weights of the ion ground states, respectively $U_{\text{Na II}} = 1$, $U_{\text{Na III}} = 6$ (Allen 1976);

- the sodium abundance is $A_{\text{Na}} = N_{\text{Na}}/N_H = 1.74 \times 10^{-6}$ (Asplund et al. 2009).

3.5 Line broadening

The Voigt function $H(a, v)$ describes the extinction profile shape and is defined by:

$$H(a, v) \equiv \frac{a}{\pi} \int_{-\infty}^{+\infty} \frac{e^{-y^2}}{(v-y)^2 + a^2} \, dy \tag{18}$$

$$y = \frac{\xi}{c} \frac{\lambda_0}{\Delta\lambda_D} \tag{19}$$

$$v = \frac{\lambda - \lambda_0}{\Delta\lambda_D} \tag{20}$$

$$a = \frac{\lambda^2}{4\pi c} \frac{\gamma}{\Delta\lambda_D}, \tag{21}$$

where ξ is velocity along the line of sight and a the damping parameter. The Dopplerwidth $\Delta\nu_D$ is not only set by the thermal broadening but includes also the microturbulent "fudge parameter" v_t (column v_t in FALC Tables 3–4) through defining it as:

$$\Delta\lambda_D \equiv \frac{\lambda_0}{c} \sqrt{\frac{2kT}{m} + v_t^2} \tag{22}$$

where m is the mass of the line-causing particle in gram, for sodium $m_{Na} = 22.99 \times 1.6605 \times 10^{-24}$ g (http://physics.nist.gov/cuu/Constants/index.html).

The Voigt function represents the convolution (smearing) of a Gauss profile with a Lorentz profile and therefore has a Gaussian shape close to line center ($v = 0$) due to the thermal Doppler shifts ("Doppler core") and extended Lorentzian wings due to disturbances by other particles ("damping wings"). A reasonable approximation is obtained by taking the sum rather than the convolution of the two profiles:

$$H(a, v) \approx e^{-v^2} + \frac{a}{\sqrt{\pi} \, v^2}. \tag{23}$$

$H(a, v)$ is available in IDL as function `VOIGT(a,v)`, but it works correctly only for positive `v`, so use it with `abs(v)`.

The damping parameter a may be approximated by taking only Van der Waals broadening into account in (21). Figure 11.6 of Gray (1992) shows this by comparing Van der Waals broadening with natural broadening and Stark broadening for the Na I D lines throughout a solar radiative-equilibrium model. However, since the FALC model reaches higher we might also add in natural broadening with:

$$\gamma_{rad} = A_{ul} = 6.67 \times 10^{13} \frac{g_l}{g_u} \frac{f_{lu}}{\lambda^2} \; s^{-1} \tag{24}$$

for λ in nm.

The classical evaluation recipe of Van der Waals broadening by Unsöld 1955 is (cf. Warner 1967)

$$\log \gamma_{vdW} \approx 6.33 + 0.4 \log(\overline{r_u^2} - \overline{r_l^2}) + \log P_g - 0.7 \log T, \tag{25}$$

where the mean square radii $\overline{r^2}$ of the upper and lower level are usually estimated from the hydrogenic approximation of Bates & Damgaard (1948)

$$\overline{r^2} = \frac{n^{*2}}{2Z^2} \left(5n^{*2} + 1 - 3l(l+1)\right) \tag{26}$$

23

with $\overline{r^2}$ measured in atomic units, l the angular quantum number of the level and n^* its effective (hydrogen-like) principal quantum number given by

$$n^{*2} = R \frac{Z^2}{E_\infty - E_n} \qquad (27)$$

in which the Rydberg constant $R = 13.6\,\text{eV} = 2.18 \times 10^{-11}$ erg, Z is the ionization stage ($Z = 1$ for Na I, $Z = 2$ for Na II, etc) and $E_\infty - E_n$ is the ionization energy from the level (compute the excitation energy of the upper level from the line-center wavenumber). The common Na I D_1 and Na I D_2 lower level ($3s\,^2S_{1/2}$) has $l = 0$, the upper levels ($3p\,^2P^o_{1/2}$ and $3p\,^2P^o_{3/2}$) have $l = 1$.

3.6 Implementation

- Implement the above into a function that returns the line extinction at all heights of the FALC atmosphere, for example `NaD1_ext(wav,temp,eldens,nhyd,vmicro)`. It is best to make this a set of subroutines that process the atmospheric arrays in one go, without "`for ih=0,nh-1 do begin`" unrolling because that results in much slower execution.

- You might prefer to generalize this effort to any Fraunhofer line instead of making a special function for this particular line only. This then involves automation of getting the partition functions of all atom stages of interest for use in a more general Saha function. You might check out the ancient IDL routines and atomic data file at `https://github.com/aasensio/lte/tree/master/idl`, based on the yet more ancient Fortran routines of Wittmann (1974). I used them in my own `ltelib`.

3.7 Computed Na D_1 line profile

You are now ready to model the solar Na I D_1 line.

- Add the Na I D_1 line extinction to the continuous extinction in your integration code from the previous exercise and compute the disk-center Na I D_1 profile.

- Compare the computed line profile to the observed line profile and discuss the differences. Explain why your computed profile has a line-center reversal.

- Traditionally, stellar abundance determiners vary a collisional enhancement factor E by which γ_{vdW} is multiplied in ad-hoc "fudge-factor" fashion in order to obtain a better fit of the line wings. You may try such, or better broadening recipes from Paul Barklem at `http://www.astro.uu.se/~barklem`.

3.8 Discussion

Your code constitutes a 1960–style solar line synthesis program which is easily generalized to other atomic species. However, your computed Na I D_1 line core doesn't reach as deep as the observed one which does not show an intensity reversal. This discrepancy shows that the assumption of LTE breaks down for the core of this line. No wonder, the solar Na I D lines are strong scatterers (small ε) with large NLTE source function sensitivity to J_λ rather than to B_λ at heights around the temperature minimum where their cores originate. In fact, their formation closely follows the two-level atom description for resonance scattering in which both J_λ and S_λ drop down to a value of only about $\sqrt{\varepsilon}\,B_\lambda$ at the surface, displaying standard NLTE scattering behavior. Thus, it is time for *"Stellar Spectra C: NLTE Line Formation"* — but I still have to complete this sequel set of exercises. It will include parts of former practicals at Utrecht University that remain available here.

References

Abramowitz, M. & Stegun, I. A. 1965, Handbook of mathematical functions (National Bureau of Standards) (`1965hmfw.book.....A`)

Allen, C. W. 1976, Astrophysical Quantities (3rd edition, Athlone Press) (`1976asqu.book.....A`)

Aller, L. H., Appenzeller, I., Baschek, B., et al., eds. 1982, Landolt-Bornstein, Group 6: Astronomy (`1982lbg6.conf.....A`)

Anders, E. & Grevesse, N. 1989, Geochim. Cosmochim. Acta, 53, 197 (`1989GeCoA..53..197A`)

Asplund, M., Grevesse, N., Sauval, A. J., & Scott, P. 2009, ARA&A, 47, 481 (`2009ARA&A..47..481A`)

Avrett, E. H. & Loeser, R. 2008, ApJS, 175, 229 (`2008ApJS..175..229A`)

Bates, D. R. & Damgaard, A. 1948, ApJ, 107, 383 (`1948ApJ...107..383B`)

Brault, J. W. 1980, in Future Solar and Optical Observations Needs and Constraints, ed. G. Godoli, G. Noci, & A. Righini, 33 (`1980fsoo.conf...33B`)

Chandrasekhar, S. & Breen, F. H. 1946, ApJ, 104, 430 (`1946ApJ...104..430C`)

Eddington, A. S. 1926, The Internal Constitution of the Stars (Cambridge University Press) (`1926ics..book.....E`)

Engvold, O. 1977, Phys. Scrip., 16, 48 (`1977PhyS...16...48E`)

Fontenla, J. M., Avrett, E. H., & Loeser, R. 1993, ApJ, 406, 319 (`1993ApJ...406..319F`)

Gray, D. F. 1992, The Observation and Analysis of Stellar Photospheres. (2nd edition, Cambridge University Press) (`1992oasp.book.....G`)

Gray, D. F. 2005, The Observation and Analysis of Stellar Photospheres (3rd edition, Cambridge University Press) (`2005oasp.book.....G`)

Hearnshaw, J. B. 1986, The analysis of starlight (Cambridge University Press) (`1986asoh.book.....H`)

Moore, C. E., Minnaert, M. G. J., & Houtgast, J. 1966, The solar spectrum 2935 Å to 8770 Å (NBS) (`1966sst..book.....M`)

Neckel, H. 1999, Sol. Phys., 184, 421 (`1999SoPh..184..421N`)

Novotny, E. 1973, Introduction to stellar atmospheres and interiors (Oxford University Press) (`1973itsa.book.....N`)

Pannekoek, A. 1930, MNRAS, 91, 139 (`1930MNRAS..91..139P`)

Parker, E. N. 1958, ApJ, 128, 664 (`1958ApJ...128..664P`)

Press, W. H., Flannery, B. P., & Teukolsky, S. A. 1986, Numerical recipes. The art of scientific computing (Cambridge University Press) (`1986nras.book.....P`)

Ulrich, R. K. 1970, ApJ, 162, 993 (`1970ApJ...162..993U`)

Unsöld, A. 1955, Physik der Sternatmosphären (2. Auflage, Springer) (`1955QB461.U55......`)

Vernazza, J. E., Avrett, E. H., & Loeser, R. 1981, Astrophys. J. Suppl. Ser., 45, 635 (`VALIII`)

Vernazza, J. E., Avrett, E. H., & Loeser, R. 1981, ApJS, 45, 635 (`1981ApJS...45..635V`)

Wallace, L., Hinkle, K., & Livingston, W. 1998, An atlas of the spectrum of the solar photosphere from 13,500 to 28,000 cm-1 (3570 to 7405 A) (`1998assp.book.....W`)

Warner, B. 1967, MNRAS, 136, 381 (`1967MNRAS.136..381W`)

Wildt, R. 1939, ApJ, 89, 295 (`1939ApJ....89..295W`)

Wittmann, A. 1974, Sol. Phys., 35, 11 (`1974SoPh...35...11W`)